BULLETIN OF THE POLISH ACADEMY OF SCIENCES
TECHNICAL SCIENCES, Vol. 59, No. 4, 2011
DOI: 10.2478/v10175-011-0063-5

CM voltage compensation in AC/DC/AC interfaces for smart grids

R. SMOLEŃSKI*, M. JARNUT, G. BENYSEK, and A. KEMPSKI

University of Zielona Góra, Institute of Electrical Engineering, 50 Podgórna St., 65-246 Zielona Góra, Poland

Abstract. In this paper the results of research connected with common mode (CM) interference generated by four-quadrant frequency converters and effective methods of CM voltage compensation are presented. The obtained results show that conducted CM interference generated by these converters in a low voltage (LV) grid can be transferred by means of parasitic couplings into a medium voltage (MV) network and can be observed at distant points under overhead MV lines. The compensation of the CM voltage sources on both the input and the output sides of the AC/DC/AC converter using proposed arrangement of compensators significantly reduces unwanted, EMC related, side effects accompanying the application of AC/DC/AC interfaces in Smart Grids.

Key words: electromagnetic compatibility, conducted interferences, distributed system, power electronic interface.

1. Introduction

In distributed generation systems power electronic converters are applied as interfaces in general to:

- matching parameters and coupling of distributed sources with power lines or local end-users, and controlling consumption of EE with these sources, Fig. 1,
- matching parameters and coupling of energy storage with power lines, and controlling the exchange of energy between storage systems and power lines,
- improving the quality of the power supply, among other things: compensation of sags and swells, asymmetry and distortions of supply voltage, as well as compensation for distortion, asymmetry and phase shift in load current [1–3].

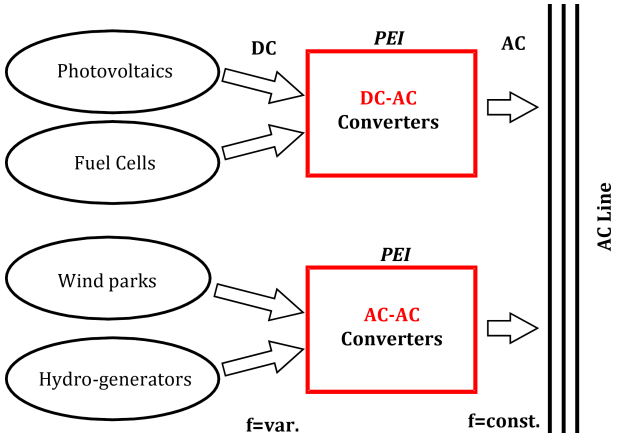

Fig. 1. Power-electronics in alternative generation systems

The small electrical energy sources dispersed in electrical power systems (EPS) referred as distributed generation (DG) are one of the most significant parts of future grids – Smart Grids [1–10]. Four-quadrant frequency converters are currently commonly applied in novel asynchronous drives and are increasingly being used in distributed power generation systems as power electronic interfaces (PEI) for asynchronous and permanent magnet variable speed generators [11], Fig. 2. The main circuit of the four-quadrant frequency converter consists of two IGBT based three-phase bridges and an intermediate circuit allowing two-way energy flow and four-quadrant operation.

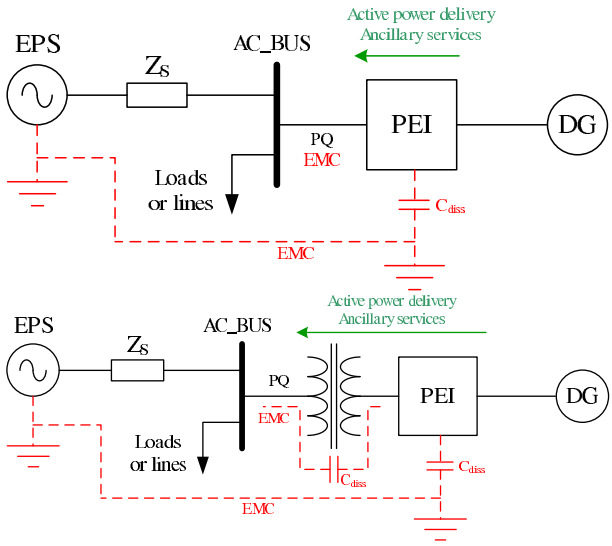

Fig. 2. Low voltage distributed generation systems

1.1. CM voltage related problems. The impulse energy conversion by means of two fully controlled three phase full-bridge converters causes that voltage interference sources appear on the both a line and a load side of the converter. These sources may lead to the problems with internal and external electromagnetic compatibility. The converter on the line side might force a flow of the significant electromagnetic interference EMI currents, while the output inverter, assuring the operation of the generator in regenerative braking quadrant, introduces electrical asymmetry that causes a flow of EMI currents [12] on the motor side and is the reason for

*e-mail: R.Smolenski@iee.uz.zgora.pl

the appearance of electric discharge machining (EDM) currents that may bring about premature damage of the bearing races. Figure 3 shows the pictures of the 500 kW asynchronous generator bearing with typical race damages caused by EDM currents [13].

The results of the statistical analysis presented in previous paper [13] have shown that the inverter switching frequency as well as a selection of the filter type have a significant influence on the amplitude and frequency of the EDM current appearance. These factors determine a life of generator bearings. Figures 4 and 5 show three-dimensional histograms of the EDM current amplitudes and awaiting times to punctures for different inverter switching frequencies and for various inductive filters.

Fig. 3. Bearing race damages caused by EDM currents

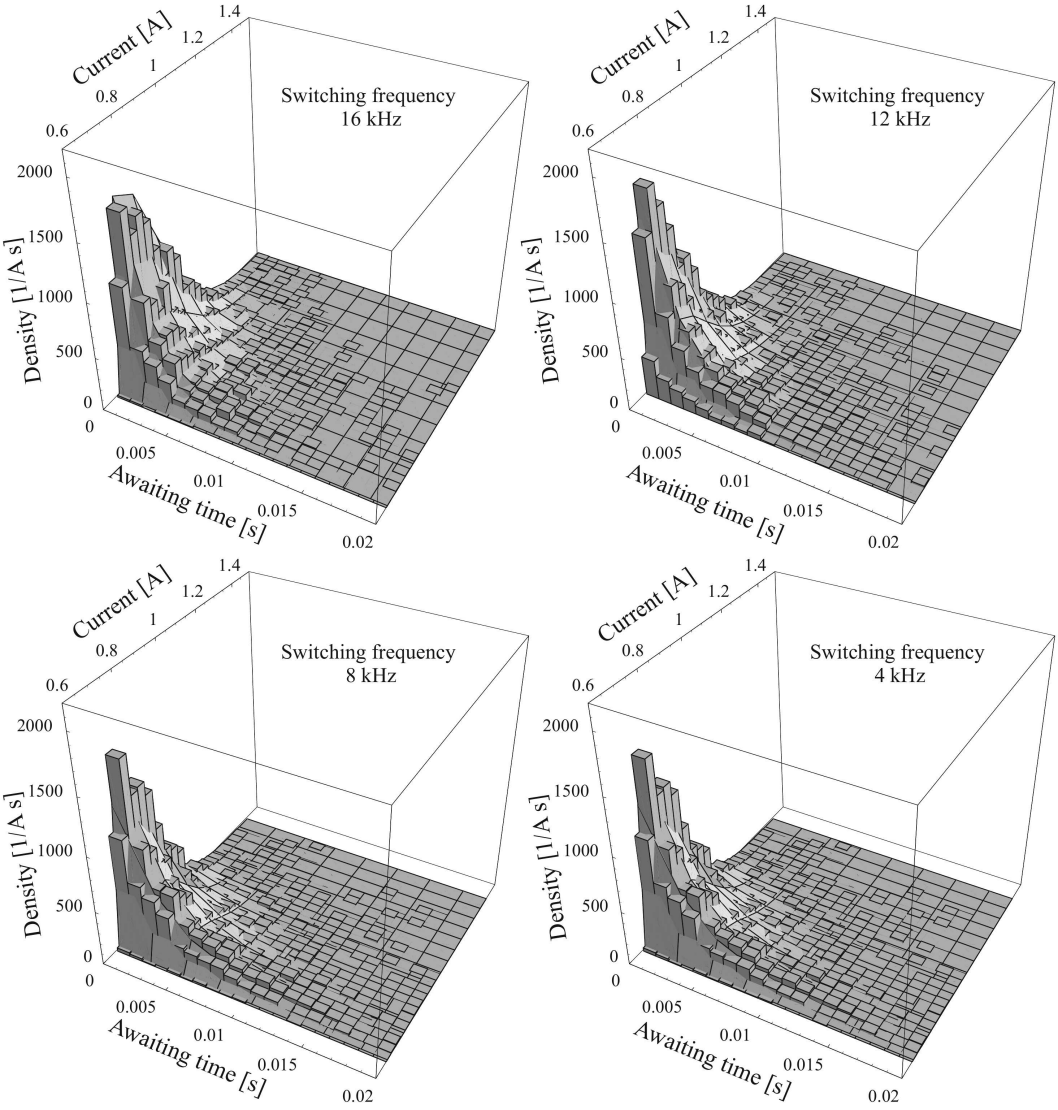

Fig. 4. 3D distributions of EDM currents for various switching frequencies

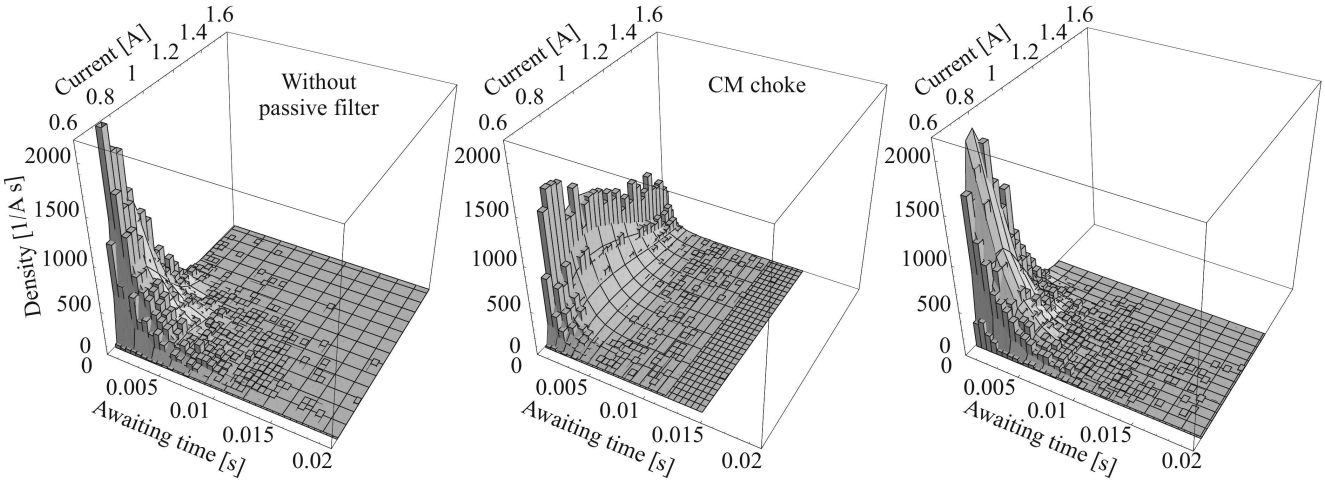

Fig. 5. 3D distributions of EDM currents in a drive: without filters, with CM choke and CM transformer

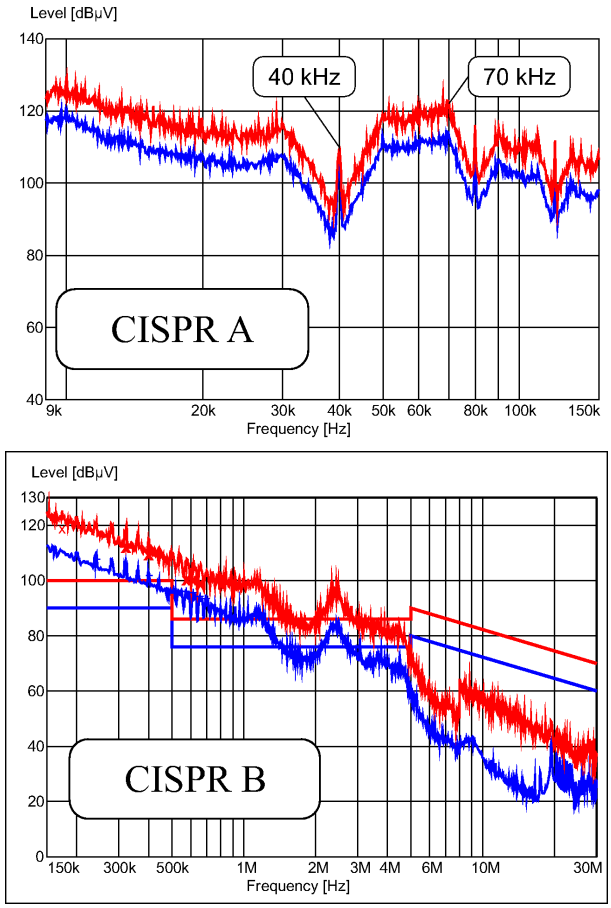

Fig. 6. Conducted EMI spectra in CISPR A and CISPR B frequency ranges

A relatively high level of the generated interferences, especially in CISPR A frequency band and observed malfunctions of the electronic equipment caused by the converter in relatively distant circuits forced authors to carry out the researches of the interference penetration depth into the local grid. The commercially available 25 kW four-quadrant frequency converter with 10 kW asynchronous generator have been used in the interference flow researches. Preliminary measurements have been done in normalized system comprised of the EMI receiver and Line Impedance Stabilization Network (LISN). Figure 6 shows results of the measurements using peak and average detectors and a typical intermediate frequency bandwidth (IF BW) equal to 200 Hz and 9 kHz for CISPR A and CISPR B frequency range, respectively.

2. Flow of the CM interferences generated by AC/DC/AC converter in local grid

In order to assess the interference penetration depth into electric grid CM interference currents have been measured in PE wire of the converter supplied directly from a local grid without LISN. Results of the performed measurement in CISPR A frequency band is presented in Fig. 7. The shape of the CM current indicates that CM mode noises are mainly responsible for the high level of the emission introduced by the investigated converter.

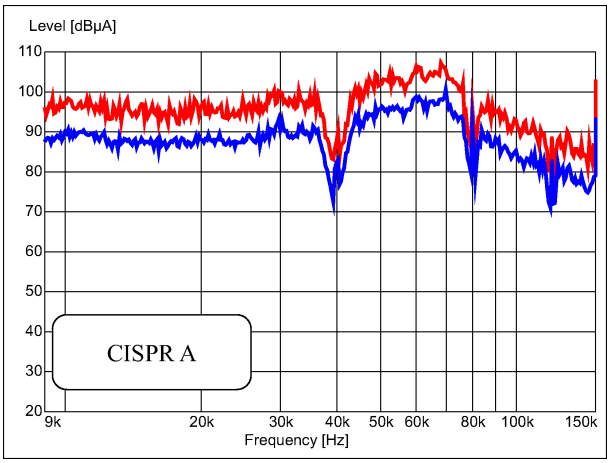

Fig. 7. Conducted EMI spectrum for CISPR A frequency range

Analysis of the interference penetration depth was possible thanks to the characteristic shape of the spectrum generated

by the converter [14–16]. The spectrum envelope is typical for damped oscillatory mode waveforms of frequency equal to 70 kHz that is formed in resonant circuits created by input line reactors, impedance of the grid and heat sink-to-DC link capacitances, whereas the shape of the spectrum near frequencies that are multiple of the 40 kHz is connected with the frequency of the sample and hold (S&H) transistor switching synchronization signal and attenuation of the input resonant filter.

Figure 8 presents the electrical installation scheme in laboratory halls with depicted cable lengths and points where interference voltage measurements, at frequency equal to 70 kHz with IF BW = 200 Hz, have been carried out.

Figure 9 shows results of the measurements carried out in points depicted in Fig. 8. In each measuring point 100 measurements at the 70 kHz frequency lasting 1 s using quasi-peak detector have been taken. The measurements have been done for switched-off and switched-on converter. The results are presented in a form of the box-and-whisker plots with measured individual values marked with dots. In spite of the local grid extensiveness, the operation of the converter caused significant increase of the interference levels in all of the measuring points. The increase of the interference levels strongly depends on the distance from the converter to the measuring point.

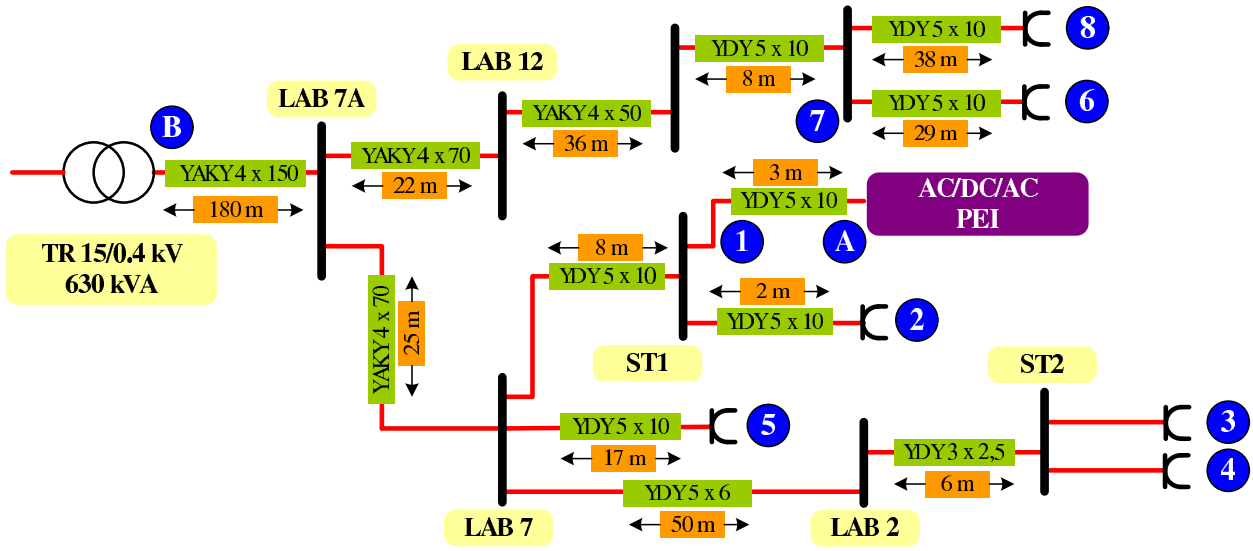

Fig. 8. Electric grid scheme with depicted measuring points

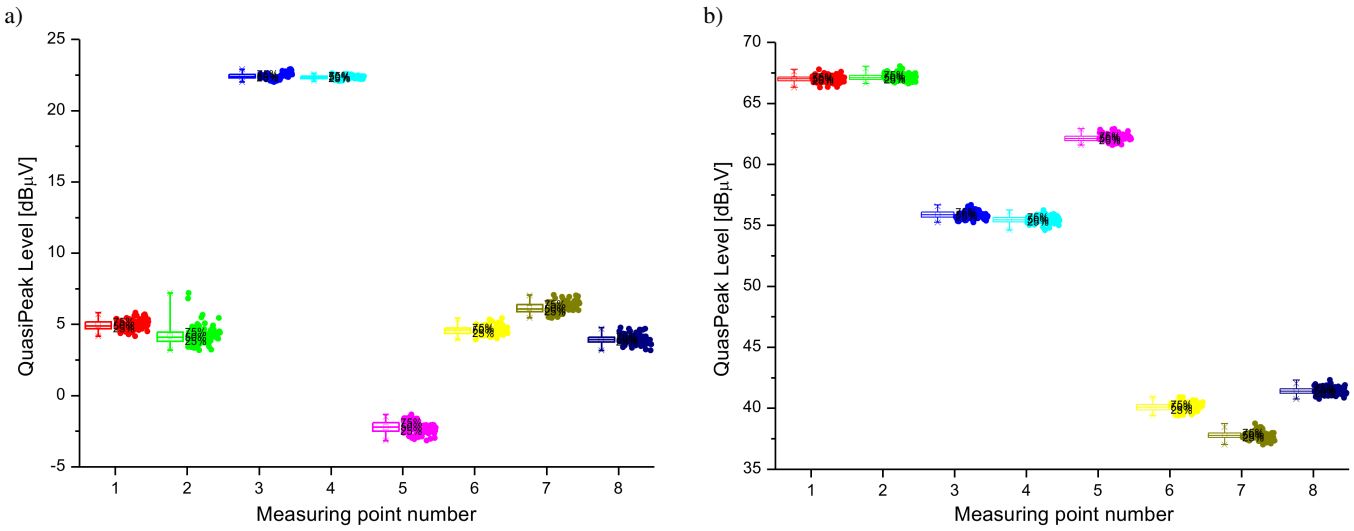

Fig. 9. Box-and-whisker plot of quasi-peak detector measurements for: a) interface turned off, b) interface turned on

Figure 10 shows the spectrum of the CM current measured using a current probe in the PE wire of the power supply cable that supplies a laboratory. A measuring point was located at a transformer station near a common PE bus more than 200 m away from the interference source. Figure 10a shows the spectrum of background noise in cable PE wire and Fig. 10b shows the spectrum of CM current measured in the same point during a converter operation. The level of the CM interference increases significantly. At a frequency of 60 kHz, which constitutes the main oscillatory mode of the current, the level of interference increased 100 times (40 dB) compared to background interference. The observed level is only 20 dB lower in comparison with interference measured in the PE wire near the converter, in spite of the existence of many alternative paths for the interference flow in the laboratory hall.

a)

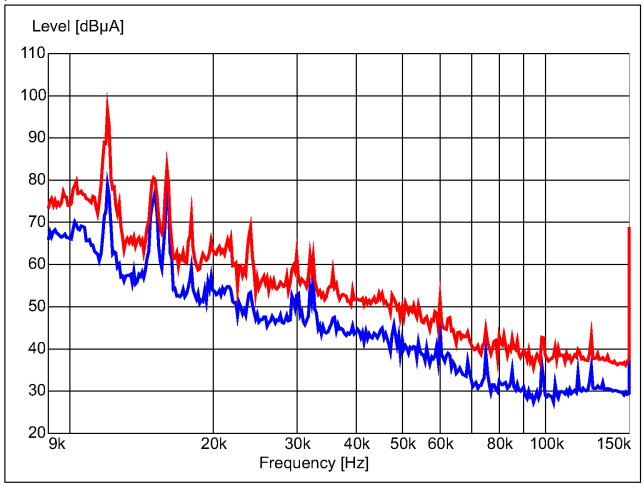

b)

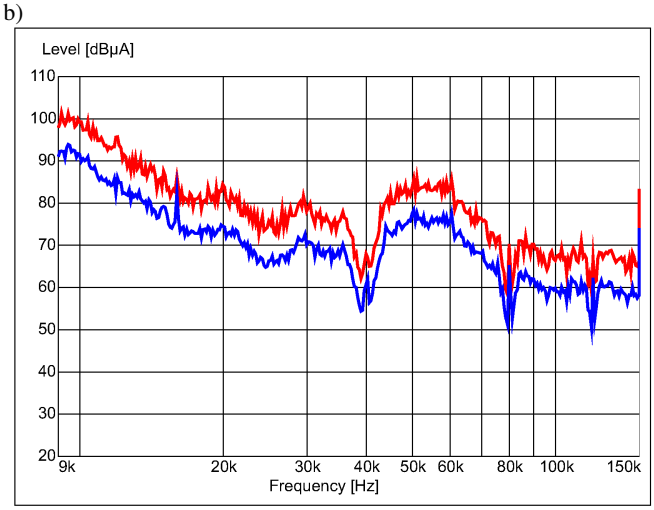

Fig. 10. Spectra of current in PE wire of power cable at transformer terminal for: a) switched off converter, b) switched on converter

As it has been stated in previous paper [14] an identification of the higher frequency interferences is difficult due to the modification of the resulting spectrum by strongly nonlinear impedance of the interference current paths. Figure 11 shows results of the CM impedance module measurements for different lengths of the YAKY 4×25 mm^2 power cable. With increasing length of the cable the resonant frequencies in lower frequency ranges have to be taken into account.

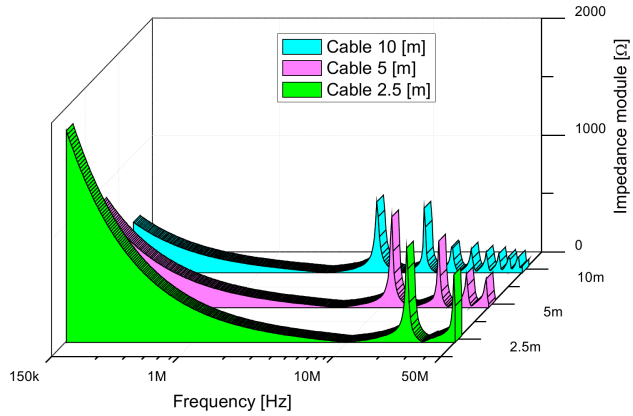

Fig. 11. CM impedance module of YAKY 4×25 mm^2 cable: 2.5 m, 5 m and 10 m long

3. Measurements of interferences in MV overhead lines introduced by AC/DC/AC interfaces connected to LV grid

Further researches concerning interference spread over a distribution system were carried out in an urban type transformer station and under overhead MV lines in points depicted in Fig. 12. The AC/DC/AC interface with an asynchronous generator was connected to low voltage side of the 160 kVA power transformer.

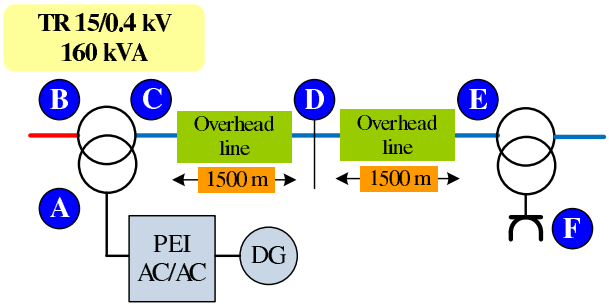

Fig. 12. MV and LV electric grid scheme with depicted measuring points

The need to carry out research of conducted electromagnetic interferences in medium voltage (MV) grids forced the application of the field measuring method. The active loop antenna was used for measuring interference penetration depth into the MV grid. It is important to note that the LV and the MV sides of the transformer were located at relatively distant points on opposite sides of the building. The presented experimental results show that EMI introduced by the converter, in systems presented in Fig. 2, is transferred by parasitic capacitive couplings onto the MV side of the transformer (not according to the transformer ratio). In this case the transformer cannot be treated as an attenuating device for high frequency interference.

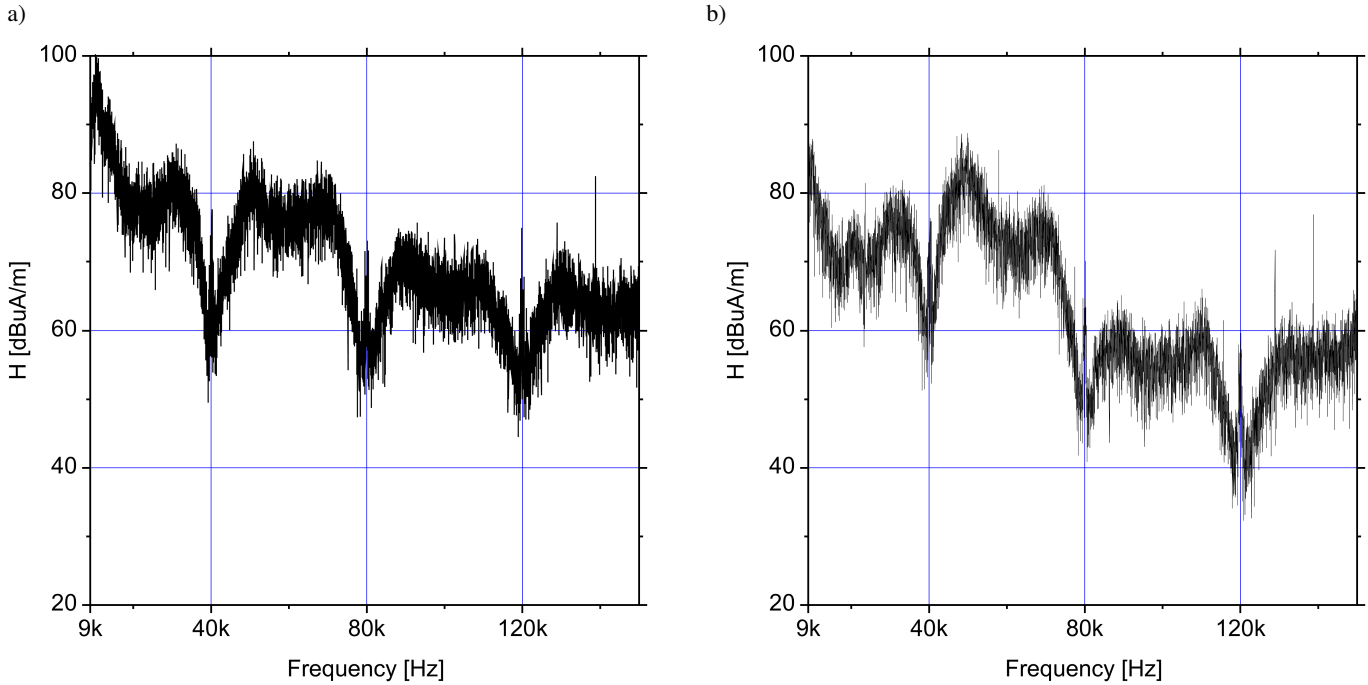

Fig. 13. Magnetic field strength on both sides of power transformer: a) low voltage side (point A), b) medium voltage side (point B)

Figure 13 shows the results of magnetic field strength measurements in the power transformer station on both low and medium voltage sides (points A and B).

Further investigations were performed under overhead MV lines. The first measurement was taken 20 m away from transformer station (point C). The second measuring point was located under an overhead MV line 1500 m (point D) and third 3000 m away from the transformer station near a second transformer station (point E). In each case the loop antenna was oriented along the lines in order to assure maximum level of interference measured in a near field, Fig. 14.

Figure 15 shows the magnetic field measured under MV overhead lines 20 m, 1500 m and 3000 m away from the transformer station during AC/DC/AC interface operation and background interference measured in point E when PEI was switched off. The specific frequencies introduced by converter can be easily identified.

Additionally, the measurements of the interference voltages on the LV side of the second transformer station have been performed. Figure 16 shows an increase of interference caused by the converter in comparison with background interference measured in socket (point F) on the LV side of the transformer station located 3000 m away from the source of the interferences. Both transformer stations are connected only by means of the MV overhead lines. In presented spectrum we can observe 20 dB increase of the interference level, during operation of the converter located in distant circuit not connected by means of LV grid, in a comparison with a background noise.

Fig. 14. Magnetic field measurement under overhead MV line

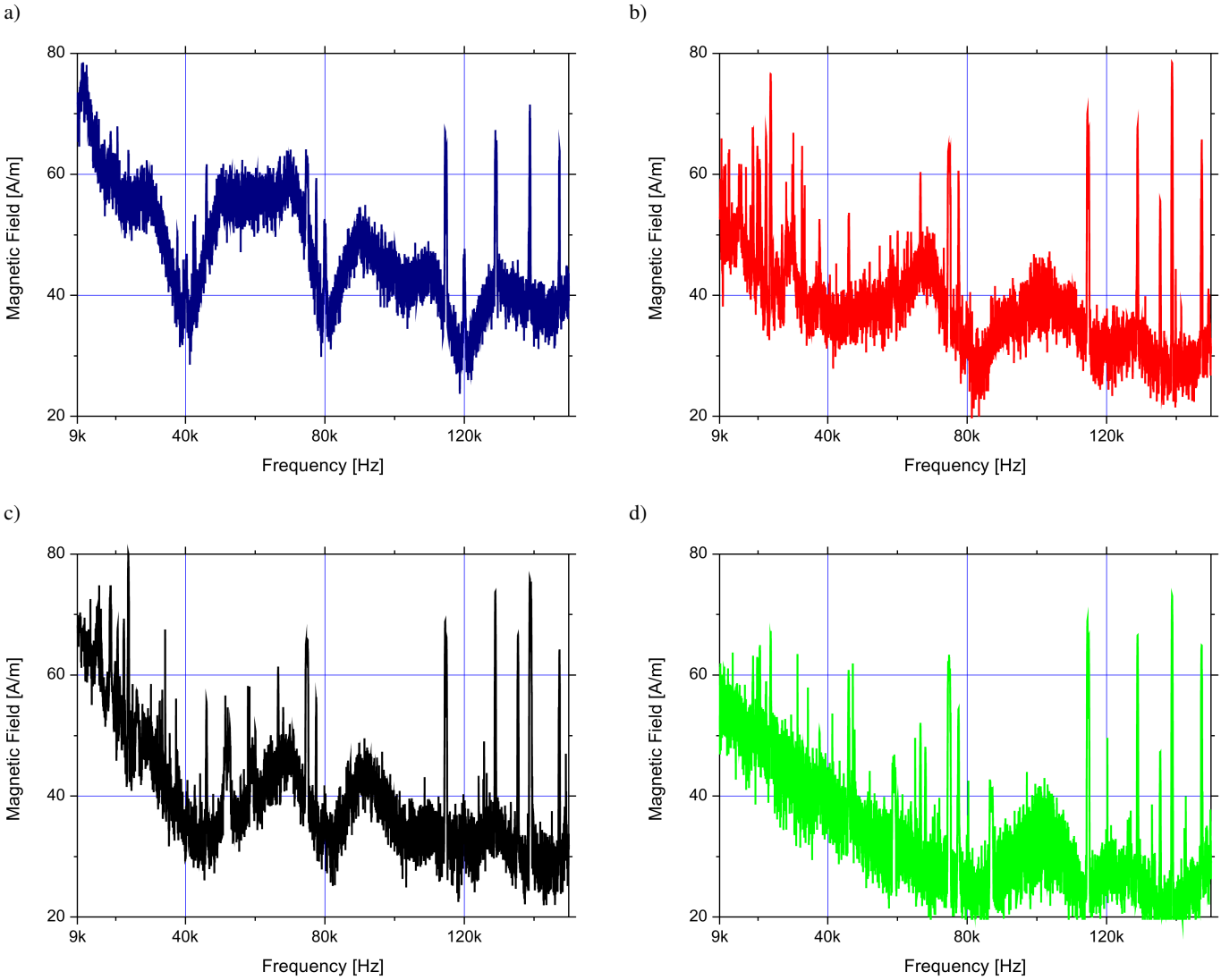

Fig. 15. Magnetic field strength under MV overhead lines: a) 20 m away from station, b) 1500 m away from station, c) 3000 m away from station, d) background noise

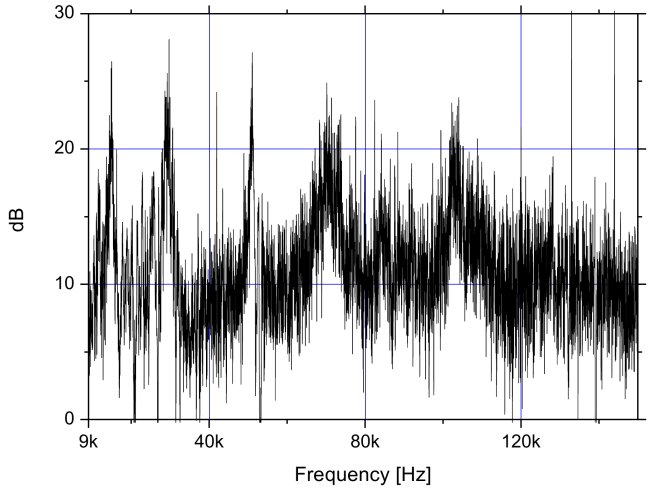

Fig. 16. Increase of interferences caused by converter measured in socket (point F)

4. Passive CM voltage compensation in AC/DC/AC PEI

A typical approach to conducted EMI reduction [17–21] bases on the application of the CM and DM filters that increase the impedance of the EMI current paths in conducted EMI frequency range. However, these solutions may bring about many side effects [9, 12] such as creation of various resonant frequencies in system with uncontrolled paths for the passage of EMI currents generated in nearby circuits, lowering of the path damping factor due to introduction of additional series inductance, increasing of the EDM current amplitudes with lowered awaiting time to puncture Fig. 5.

The complex solution for EDM current problems as well as the high level of EMI currents generated in input and output circuits of the of the converter is a cancellation of the interference sources at the input and output of the converter. The cancellation might be provided by an application of active and passive CM voltage compensators [22–27]. The passive compensator concept bases on the creation of the voltage drop, that is equal to the compensated CM voltage, on the CM choke [22]. However, as it has been proved in our previous paper [15] the application area of this solution is limited to frequency converters with diode rectifiers. The passive CM compensator assures compensation with respect to the plus or minus DC bus points. In a case of controlled rectifier, transistors' switching cause high level ripples in DC bus-to-ground voltages. In these circumstances the compensation with respect to DC bus points makes the output passive compensator ineffective. Figure 17 shows voltages of the DC buses with respect to the ground. The shapes of the waveforms are formed by the implemented control algorithm of the rectifier and an additional oscillation caused by a voltage drop across the DC-link-to-heat-sink capacitance. Nevertheless, the DC-link voltage is constant, as expected.

We have not found any filter to compensate the DC link-to-ground voltage ripples in the subject matter literature. Figure 18 shows the proposed filter arrangement for compensation of the DC link-to-ground voltage ripples caused by the active rectifier that has been developed analogically to the CM voltage filter proposed by Akagi for compensation of a CM voltage generated by an inverter.

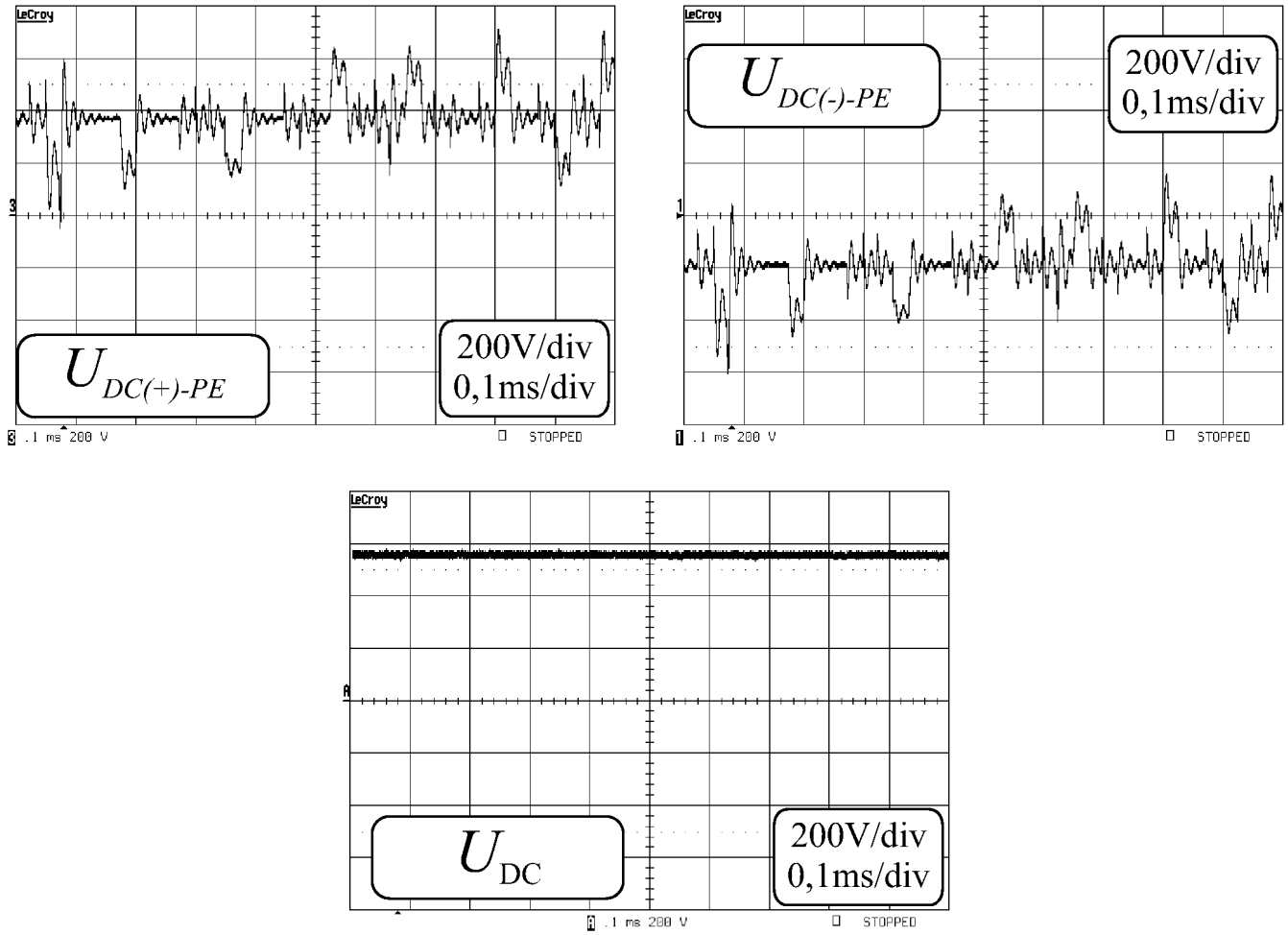

Fig. 17. Voltages of DC buses and DC link voltage (system without filters)

Figure 19 shows simulation results taken in system presented in Fig. 18 for both without and with filter positions. The effectiveness of this solution was confirmed both in simulation ($U_{DC(-)-PE}$) and experimentally. However, the placement of the CM choke in DC link causes high overvoltages on the rectifier's transistors (U_{CE}) and additionally increases significantly the differential mode impedance of the DC buses.

The analysis of the CM path on the line side of the 4-quadrant converter enabled the development of the filter possessing the same compensating properties without the above mentioned drawbacks. Figure 20 shows the proposed and patented by the authors compensator arrangement. The two-winding CM choke in the DC bus has been replaced by the three-phase CM choke on the line side of the converter. In this case the CM path remains unchanged, enabling the compensation of the DC-link-to-ground voltage ripples.

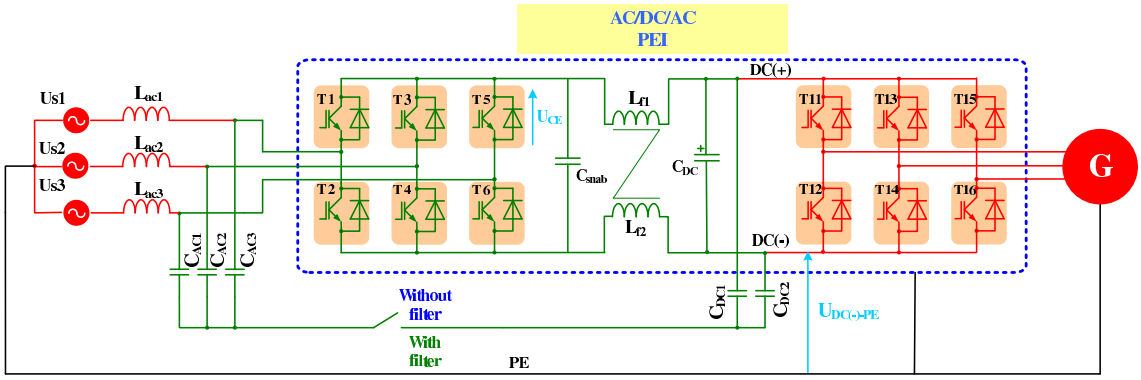

Fig. 18. Compensator of DC link-to-ground voltage ripples with CM choke in DC link

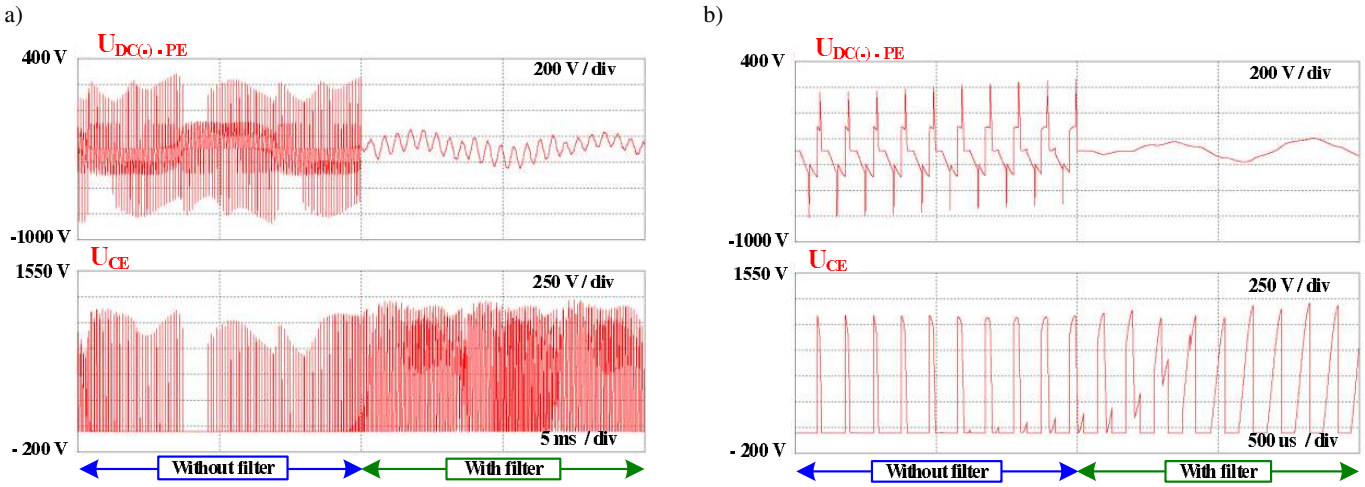

Fig. 19. Simulation waveforms of DC link-to-ground voltage ripples and collector-emitter voltages with and without filter: a) original view, b) magnified view

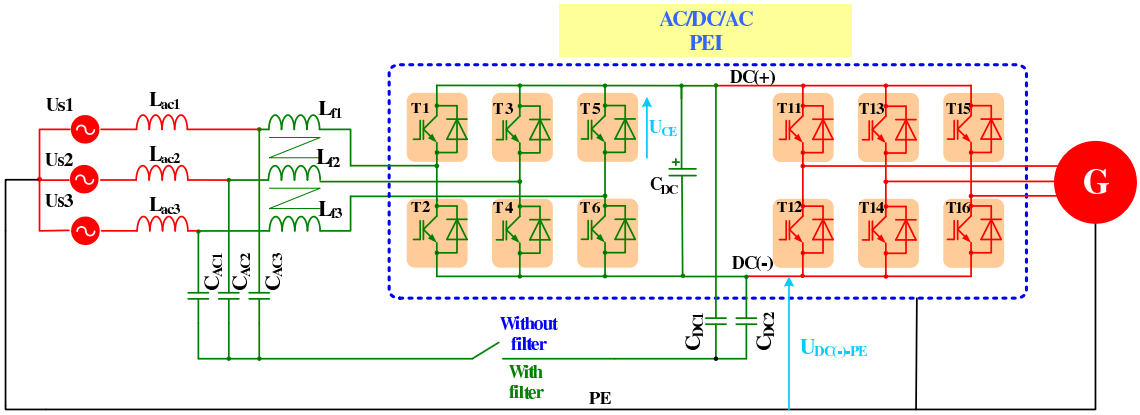

Fig. 20. Compensator of DC link-to-ground voltage ripples with three-phase input CM choke

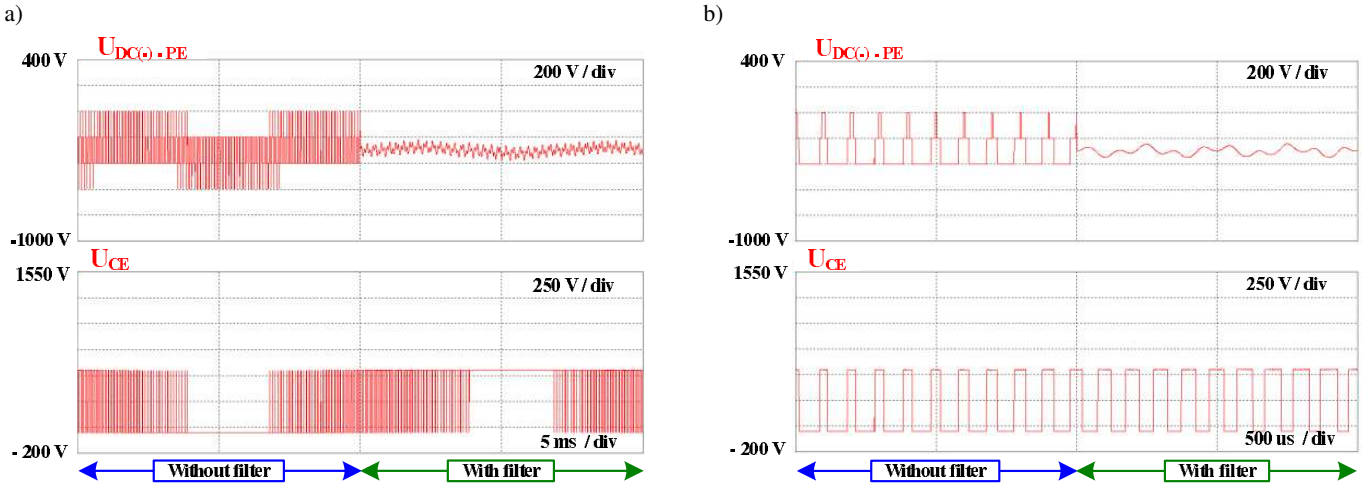

Fig. 21. Simulation waveforms of DC link-to-ground voltage ripples and collector-emitter voltages with and without filter: a) original view, b) magnified view

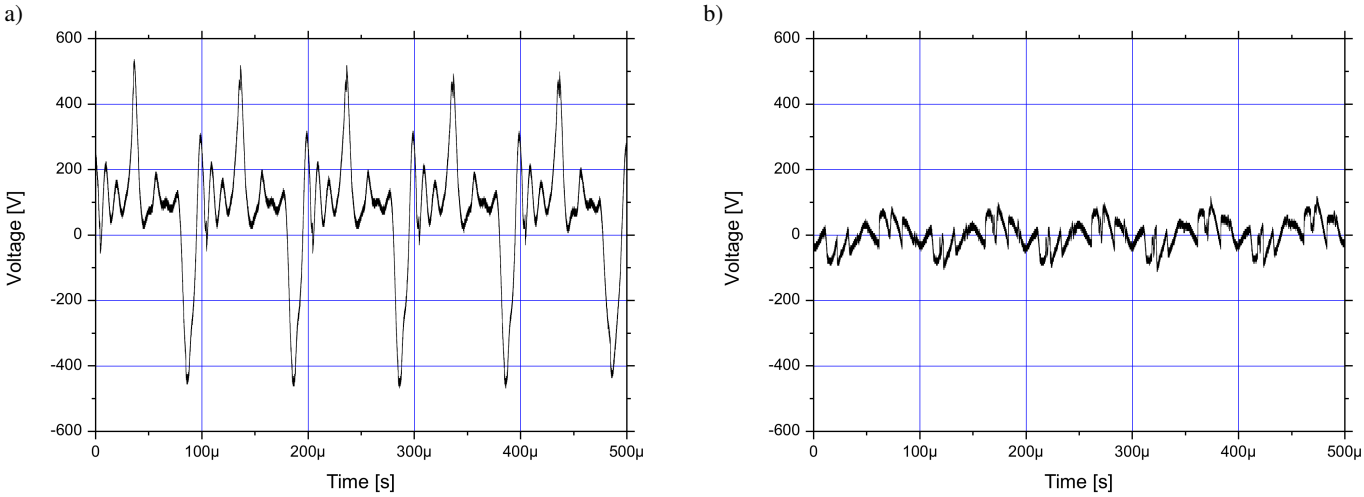

Fig. 22. DC-link-to-ground voltage ripples in power electronic interface: a) without compensator, b) with compensator

Figure 21 shows simulation results taken in system presented in Fig. 20 for both without and with filter positions. The filter significantly reduces the DC link-to-ground voltage ripples ($U_{DC(-)-PE}$) without causing of the overvoltages on transistors (U_{CE}).

Figure 22 shows the experimental waveforms of the DC-link-to-ground voltage ripples in the system consisting in a 4-quadrant frequency converter and asynchronous generator with and without the compensator shown in Fig. 20. The significant reduction of the voltage ripples results in a possibility of a successful application of the output filter providing compensation of the CM voltage caused by an inverter with respect to a DC bus assuring low interference level on the generator side and zero EDM currents.

5. Conclusions

Smart grid applications of power electronics require the connection of susceptible control and communications electronic equipment to high emission power electronic converters. This makes in-depth EMC analyses essential for ensuring system reliability. The assurance of electromagnetic compatibility seems to be one of the most important factors conditioning the development of distributed power systems.

The experimental results have shown that interferences caused by a four-quadrant converter, often used as an interface in distributed generation systems, can reach a distant point in the local low voltage grid.

The supplementary magnetic field measurements have shown that interference can be transferred by parasitic couplings on the medium voltage side of the transformer. The application of the field measuring techniques for conducted EMI frequency range allows investigations of the EMI flow in LV distributed installations and MV overhead lines. The measurements have shown that the interference introduced by power electronic interfaces into LV grid can be transferred by means of parasitic couplings of a transformer (not corresponding to transformer ratio) onto a MV side. Moreover, the results of research have shown that the conducted EMI might

spread across the extensive circuits and that MV lines might be part of the conducting paths for its passage.

The application of the proposed filter, which significantly reduces DC-link-to-ground voltage ripples, results in a successful application of the output filter to assure zero CM voltage resulting from an inverter and sinusoidal line-to-line voltages. A four-quadrant frequency converter equipped with the proposed input and output filters assures significant reduction of the CM voltages on the line and generator side of the converter.

Acknowledgements. This scientific work has been financed from the scientific research resources in the years 2009–2011, referenced under research project no. N N510 333537.

REFERENCES

[1] G. Benysek and R. Strzelecki, "Modern power-electronics installations in the Polish electrical power network", *Renewable and Sustainable Energy Rev.* 15 (1), 236–251 (2011).

[2] G. Benysek, "Improvement in the efficiency of the distributed power systems", *Bull. Pol. Ac.: Tech.* 57 (4), 369–374 (2009).

[3] G. Benysek, *Improvement in the Quality of Delivery of Electrical Energy Using Power Electronics Systems*, Springer-Verlag, London, 2007.

[4] J. Wasiak and Z. Hanzelka, "Integration of distributed energy sources with electrical power grid", *Bull. Pol. Ac.: Tech.* 57 (4), 297–310 (2009).

[5] D. Schulz, "Improved grid integration of wind energy systems", *Bull. Pol. Ac.: Tech.* 57 (4), 311–316 (2009).

[6] Z. Chen, X. Zhang, and J. Pan, "An integrated inverter for a single-phase single-stage grid-connected PV system based on Z-source", *Bull. Pol. Ac.: Tech.* 55 (3), 263–272 (2007).

[7] K.J. Dyke, N. Schofield, and M. Barnes, "The impact of transport electrification on electrical networks", *IEEE Trans. on Ind. El.* 57, 3917–3926 (2010).

[8] J.R. Pillai and B.Bak-Jensen, "Integration of vehicle-to-grid in the western danish power system", *IEEE Trans. on Sustainable Energy* 2, 12–19 (2010).

[9] H. Sekyung, H. Soohee and K.Sezaki, "Development of an optimal vehicle-to-grid aggregator for frequency regulation", *IEEE Trans. on Smart Grid* 1, 65–72, (2010).

[10] L. Pieltain Fernandez, T. Gomez San Roman, R. Cossent, C. Mateo Domingo, and P. Frias, "Assessment of the impact of plug-in electric vehicles on distribution networks", *IEEE Trans. on Power Systems* 26, 206–213 (2011).

[11] A. Sikorski and A. Kuzma, "Cooperation of induction squirrel-cage generator with grid connected AC/DC/AC converter", *Bull. Pol. Ac.: Tech.* 57 (4), 317–322 (2009).

[12] Hu, J. van Bloch and R.W. De Doncker, "Typical impulses in power electronics and their EMI characteristics", *Proc. IEEE PESC*, 3021–3027 (2004).

[13] R. Smoleński, A. Kempski, and J. Bojarski, "Statistical approach to discharge bearing currents", *COMPEL: Int. J. for Computation and Mathematics in Electrical and Electronic Eng.* 29, 647–666 (2010).

[14] R. Smoleński, "Selected conducted electromagnetic interference issues in distributed power systems", *Bull. Pol. Ac.: Tech.* 57 (4), 383–394 (2009).

[15] A. Kempski, R. Strzelecki, R. Smoleński, and G. Benysek. "Suppression of conducted EMI in four-quadrant AC drive system", *IEEE-PESC Conf.* 1, CD-ROM (2003).

[16] A. Kempski, R. Smoleński, and R. Strzelecki, "Common mode current paths and their modelling in PWM inverter-fed drives", *IEEE-PESC Conf.* 1, CD-ROM (2002).

[17] Y. Han, M. Khan, L. Xu, G. Yao, L. Zhou, and C. Chen, "A new scheme for power factor correction and active filtering for six-pulse converters loads", *Bull. Pol. Ac.: Tech.* 57 (2), 157–170 (2009).

[18] S. Wang, Y.Y. Maillet, F. Wang, D. Boroyevich, and R. Burgos, "Investigation of hybrid EMI filters for common-mode EMI suppression in a motor drive system", *IEEE Trans. on Power Electronics* 25, 1034–1045 (2010).

[19] K. Mainali and R. Oruganti, "Conducted EMI mitigation techniques for switch-mode power converters: a survey", *IEEE Trans. on Power Electronics* 25, 2344–2356 (2010).

[20] P. S. Chen and Y. S. Lai, "Effective EMI filter design method for three-phase inverter based upon software noise separation", *IEEE Trans. on Power Electronics* 25, 2797–2806 (2010).

[21] M.L. Heldwein, H. Ertl, J. Biela, and J.W. Kolar, "Implementation of a Transformerless Common-Mode Active Filter for Offline Converter Systems", *IEEE Trans. on Ind. El.* 57, 1772–1786 (2010).

[22] H. Akagi, H. Hasegawa, and T. Doumoto, "Design and performance of a passive EMI filter for use with voltage source PWM inverter having sinusoidal output voltage and zero common-mode voltage", *IEEE Trans. on Power Electronics* 19, 1069–1076 (2004).

[23] H. Akagi and T. Doumoto, "A passive EMI filter for preventing high-frequency leakage current from flowing through the grounded inverter heat sink of an adjustable-speed motor drive system", *IEEE Trans. on Ind. Appl.* 41, 1215–1223 (2005).

[24] H. Akagi and S. Tamura, "A passive EMI filter for eliminating both bearing current and ground leakage current from an inverter-driven motor power electronics", *IEEE Trans. on Power Electronics* 21, 1459–1469 (2006).

[25] H. Akagi and T.A. Oe, "Specific filter for eliminating high-frequency leakage current from the grounded heat sink in a motor drive with an active front end", *IEEE Trans. on Power Electronics* 23, 763–770 (2008).

[26] H. Akagi and T. Shimizu, "Attenuation of conducted EMI emissions from an inverter-driven motor", *IEEE Trans. on Power Electronics* 23, 282–290 (2008).

[27] J. Biela, A. Wirthmueller, R. Waespe, M.L. Heldwein, K. Raggl, and J.W. Kolar, "Passive and active hybrid integrated EMI filters", *IEEE Trans. on Power Electronics* 24, 1340–1349 (2009).